

The role of Compton heating in radiation-regulated accretion on to black holes

KwangHo Park^{1*}, Massimo Ricotti², Tiziana Di Matteo¹, and Christopher S. Reynolds²

¹McWilliams Center, Carnegie Mellon University, Pittsburgh, PA 15213, USA

²Department of Astronomy, University of Maryland, College Park, MD 20740, USA

Accepted. Received 2014

ABSTRACT

We investigate the role of Compton heating in radiation-regulated accretion on to black holes from a neutral dense medium using 1D radiation-hydrodynamic simulations. We focus on the relative effects of Compton-heating and photo-heating as a function of the spectral slope α , assuming a power-law spectrum in the energy range of 13.6 eV–100 keV. While Compton heating is dominant only close to the black hole, it can reduce the accretion rate to 0.1% ($l \propto \dot{m}^2$ model)–0.01% ($l \propto \dot{m}$ model) of the Bondi accretion rate when the BH radiation is hard ($\alpha \sim 1$), where l and \dot{m} are the luminosity and accretion rate normalised by Eddington rates, respectively. The oscillatory behaviour otherwise typically seen in simulations with $\alpha > 1$, become suppressed when $\alpha \sim 1$ only for the $l \propto \dot{m}$ model. The relative importance of the Compton heating over photo-heating decreases and the oscillatory behaviour becomes stronger as the spectrum softens. When the spectrum is soft ($\alpha > 1.5$), photo-heating prevails regardless of models making the effect of Compton heating negligible. On the scale of the ionization front, where the gas supply into the Strömngren sphere from large scale is regulated, photo-heating dominates. Our simulations show consistent results with the advection-dominated accretion flow ($l \propto \dot{m}^2$) where the accretion is inefficient and the spectrum is hard ($\alpha \sim 1$).

Key words: accretion, accretion discs – black hole physics – hydrodynamics – radiative transfer – methods: numerical.

1 INTRODUCTION

A realistic estimation of an accretion rate for a black hole (BH) is of great cosmological importance. It does not only determine its cosmological growth rate of the BH, but also it is linked directly to the BH luminosity, and thus radiative-feedback effects on the neighbouring gas of the host galaxies and intergalactic medium. Commonly, the Eddington-limited Bondi–Hoyle rate (Bondi & Hoyle 1944; Bondi 1952) is used as the prescription for the accretion rates of the BHs in cosmological simulations. However, this simple BH accretion recipe is not physically motivated since the gas accretion on to BHs is regulated by radiative and mechanical feedback from the BH. Due to the feedback, the thermal and dynamical structure of the accretion flow is far more complicated than the one described by the classical Bondi accretion calculation. The radiative feedback by BHs is important when the accretion activity of the BH peaks (i.e. quasar mode of active galactic nuclei, AGN), whereas the mechanical feedback is prominent in the low-accretion state (i.e., radio mode of AGN). Additionally, the BH spectrum in high-energy X-ray is known to display different characteristics switching between *hard* and *soft* states depending on the accretion luminosity

(Miyamoto et al. 1992, 1993; Belloni et al. 2011; Begelman & Armitage 2014). Thus, understanding how the transitions of the BH spectrum are coupled with the accretion luminosity is important not only for understanding the physics of the accretion flow but also for estimating the accretion rate.

High-energy UV and X-ray photons emitted from BHs regulate the gas supply to the BH by heating and ionizing the neighbouring gas (Ostriker et al. 1976; Cowie et al. 1978; Shull 1979), as well as imposing direct radiation forces on the gas inflow (Ostriker et al. 2010; Choi et al. 2012, 2014). This induces a self-regulated feedback loop between the inflowing gas and the outflowing radiation. A series of papers by Park & Ricotti (2011, 2012, 2013) focused on the role of photo-ionization and photo-heating for BHs with a mass M_{bh} accreting from the neutral, warm ($T_{\infty} \sim 10^4$ K), and dense ($n_{\text{H},\infty} (M_{\text{bh}}/100 M_{\odot}) = 10^5\text{--}10^7 \text{ cm}^{-3}$) gas where M_{bh} is the BH mass and $n_{\text{H},\infty}$ is the gas number density. In this particular scenario, motivated by cosmological simulations of the early universe, a well-defined hot ionized bubble of gas forms around the BH that is surrounded by an optically thick and neutral gas reservoir. The ionization front (I-front) formed by high-energy photons, which is typically a few orders of magnitude larger than the classical Bondi radius ($r_{\text{B}} = GM_{\text{bh}}/c_{s,\infty}^2$, where $c_{s,\infty}$ is the sound speed of the gas), plays a critical role in regulating gas supply to

* E-mail: kwanghop@andrew.cmu.edu

the BH when the BH is at rest (Park & Ricotti 2011, 2012) or in supersonic motion (Park & Ricotti 2013). Pressure equilibrium between the neutral and ionized gas across the I-front is the key factor for explaining reductions in the accretion rate (Park & Ricotti 2011, 2012, 2013). Thus, understanding the heating mechanisms or the instabilities (Williams 1999, 2002; Mizuta et al. 2005; Whalen & Norman 2008b,a, 2011; Park et al. 2014; Ricotti 2014) inside the H II region and near the I-front that might modify the thermal structure of the Strömgen sphere is extremely important in understanding the radiation-regulated growth of the BHs.

In the physical conditions close to an accreting BH, the strong radiation field and the (ionized) gas can exchange energy directly through Compton scattering. The direction of energy exchange is such as to bring the radiation-field and gas closer to thermal equilibrium. The subsequent Compton heating (or cooling) process increases (decreases) the gas temperature to the characteristic *Compton temperature* $T_C \sim 2 \times 10^7$ K (Sazonov et al. 2004). Due to the high T_C characterizing BH accretion, Compton heating may be an important radiative feedback mechanism for the super-massive black holes (SMBHs) at the centres of elliptical galaxies, inducing strong intermittencies of the BH luminosity (Sazonov et al. 2005; Ciotti & Ostriker 2001, 2007; Ciotti et al. 2009; Novak et al. 2011, 2012; Choi et al. 2012, 2014). However, Compton heating has been commonly neglected for the case of intermediate mass black holes (IMBHs) in the mass range of 10^2 – $10^4 M_\odot$ (Milosavljević et al. 2009; Li 2011; Park & Ricotti 2011, 2012, 2013) where photo-heating is assumed to be dominant. Understanding the role of Compton heating across the BH mass range is important for building a universal BH growth model that connects IMBH and SMBHs (Ferrara et al. 2014; Natarajan 2014). Both the Compton and photo-heating rates show the same dependence on the distance from the BH being proportional to the radiation flux, while they show different dependence on the ionization fraction of the medium (e.g., Madau & Efstathiou 1999; Ciotti & Ostriker 2001). The neutral fraction of the hydrogen inside a H II region increases as a function of radius; however, the fraction of the ionized atoms is close to unity since most of the hydrogen and helium is ionized. This fact suggests that photo-heating can be relatively more efficient in heating the gas near the I-front.

In this study, we focus on the role of Compton heating relative to photo-ionization and photo-heating for the accretion on to BHs embedded in an optically thick neutral medium. The primary goal of this paper is to explore when one of the two heating mechanisms dominates over the other as a function of the hardness of the spectrum. In Section 2, we describe the numerical simulation setup. We present our results in Section 3. In Section 4, we summarize and discuss our findings.

2 METHODOLOGY

2.1 Compton heating as a function of spectral index

The Compton heating (or cooling) rate is determined by the number of scatterings $N_{\text{scatt}}(\nu)$ per unit time, and the energy exchange per interaction $\Delta E(\nu, T)$, between the high-energy photons from a BH and the electrons in the neighbouring gas medium with a gas temperature T . Under the assumption of spherical symmetry, the Compton heating rate (Γ_C) is given by:

$$\Gamma_C = \frac{\sigma_T n_e}{m_e c^2} \int_{\nu_{\min}}^{\nu_{\max}} d\nu F_\nu (h\nu - 4k_B T), \quad (1)$$

where n_e is the electron number density, and σ_T is the Thomson cross-section. The radiation flux F_ν at frequency ν in Equation (1) depends on the distance from the BH and the optical depth τ_ν , however the optical depth can be generally neglected in optically-thin situations ($F_\nu = L_\nu/4\pi r^2$) such as in the vicinity of the BH. Assuming a power-law spectrum ($F_\nu = C\nu^{-\alpha}$), the radiation flux can be expressed $F = C(\nu_{\max}^{1-\alpha} - \nu_{\min}^{1-\alpha})/(1-\alpha)$ for $\alpha \neq 1$ while $F = C \ln(\nu_{\max}/\nu_{\min})$ for $\alpha = 1$. Equation (1) can be integrated to give a simple expression:

$$\Gamma_C = F \frac{\sigma_T n_e}{m_e c^2} \left(\frac{h\nu_{\max}}{\Lambda_C} - 4k_B T \right), \quad (2)$$

where $\Lambda_C = \ln(\nu_{\max}/\nu_{\min})$ for the special case of $\alpha = 1$. In general, Λ_C can be expressed for $1 < \alpha < 2$ as

$$\Lambda_C = \left(\frac{2-\alpha}{\alpha-1} \right) \frac{\nu_{\max}^{2-\alpha} - \nu_{\min}^{2-\alpha} (\nu_{\max}/\nu_{\min})}{\nu_{\max}^{2-\alpha} - \nu_{\min}^{2-\alpha}}. \quad (3)$$

From Equation (2), the characteristic Compton temperature T_C is defined as

$$T_C \equiv \frac{h\nu_{\max}}{4k_B \Lambda_C}, \quad (4)$$

which is the temperature when the radiation field and the gas are in equilibrium state. The Compton temperature monotonically increases with the maximum photon energy $E_{\max} = h\nu_{\max}$ and decreases as a function of the spectral index α . In Fig. 1, circles and triangles show the Compton temperature as a function of the spectral index α for $h\nu_{\max} = 100$ and 30 keV respectively with the fixed $E_{\min} = 13.6$ eV. For example, with $\alpha = 1$ and $E_{\max} = 100$ keV, the Compton temperature reaches $T_C \sim 3 \times 10^7$ K, while $T_C \sim 3 \times 10^6$ K when $\alpha = 1.5$. Since T_C is approximately proportional to E_{\max} , the T_C is lower when $E_{\max} = 30$ keV. The maximum photon energy of $E_{\max} = 100$ keV is adopted since Compton scattering becomes less efficient for photons with energies above $E \sim 100$ keV, where the relativistic effects encapsulated by the Klein–Nishina correction reduce the scattering cross-section σ_T (Klein & Nishina 1929; Blumenthal 1974). In addition, the Nuclear Spectroscopic Telescope Array (NuSTAR) has shown that spectra of many (non-blazar) accreting BH systems appear to cut off at approximately 100 keV due to the physics of the accretion disk corona (Harrison et al. 2013).

Park & Ricotti (2011, 2012) found that the thermal structure of the H II region (i.e., the temperatures in and out of the Strömgen sphere) created by UV and X-ray photons from BHs determines the accretion rate. They also found that the typical temperature T_{in} at the effective accretion radius inside the Strömgen sphere is altered by the hardness of the emitted radiation (i.e., the spectral index α of the power-law spectrum). T_{in} increases with the harder spectrum, but still remains less than $\sim 10^5$ K. This results from the fact that the mean energy of the emitted photons increases with decreasing α . Since both of the Compton heating and photo-heating depend strongly on the hardness of the spectrum, the relative importance of the two heating mechanisms must be compared with the same spectral index α .

2.2 Accretion feedback models

The bolometric luminosity of a BH is $l = \eta \dot{m}$, where the luminosity and the accretion rate are normalised by the Eddington rates as $l \equiv L/L_{\text{Edd}}$ and $\dot{m} \equiv \dot{M}/\dot{M}_{\text{Edd}}$. The Eddington luminosity is $L_{\text{Edd}} = 4\pi G M_{\text{bh}} m_p c \sigma_T^{-1}$ and we define the Eddington accretion rate $\dot{M}_{\text{Edd}} \equiv L_{\text{Edd}} c^{-2}$. For a thin disc (Shakura & Sunyaev 1973) model, the radiative-efficiency is constant $\eta \sim 0.1$ and

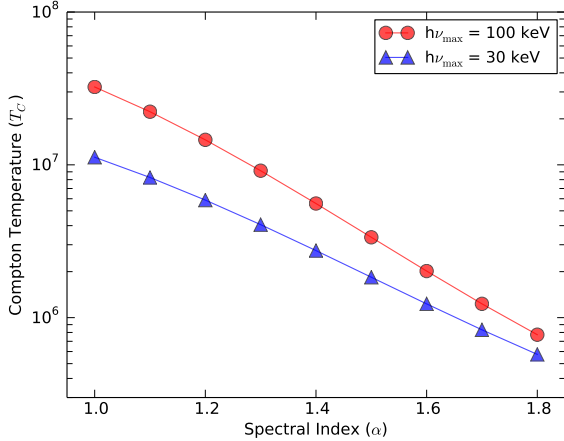


Figure 1. The Compton temperature T_C as a function of spectral index (α). Circles and triangles show T_C for the maximum energy of the photon $E_{\max} = 100$ and 30 keV, respectively. With a fixed $E_{\max} = 100$ keV, the Compton temperature is $T_C \sim 3 \times 10^7$ K for $\alpha = 1$ and monotonically decreases with increasing α , reaching $T_C \sim 3 \times 10^6$ K for $\alpha \sim 1.5$. With $E_{\max} = 30$ keV, the Compton temperature is $T_C \sim 10^7$ K at $\alpha = 1$, which is lower than the T_C for $E_{\max} = 100$ keV. The difference between T_C for different E_{\max} becomes reduced with increasing α due to the extra dependence on E_{\max} and α shown in Equation (3).

$0 < \dot{m} < \eta^{-1} \sim 10$ for Eddington-limited accretion. On the other hand, the efficiency increases as the accretion rate increases for spherical accretion or an advection-dominated accretion flow (ADAF), going as $\eta \propto \dot{m}$ (Shapiro 1973; Narayan & Yi 1995; Abramowicz et al. 1996; Park & Ostriker 2001). The ADAF model ($l \propto \dot{m}^2$) is radiatively-inefficient and is applicable when the accretion rate is low. The soft synchrotron photons from the ADAF inverse Compton scatter off the hot (~ 100 keV) electrons in the plasma and produce a hard spectrum ($\alpha = 1$) (Narayan et al. 1998). Interestingly, it has been shown that the photo-heating/ionization alone does not produce a significant difference between $l \propto \dot{m}$ and $l \propto \dot{m}^2$ models when a same spectral index α is assumed for these two models (Park & Ricotti 2011). This is due to the fact that the thermal structure inside the H II region (described by the parameter T_{in}), the key for determining the accretion rate, is not affected by the difference between the two models but significantly altered by the spectral index as explained in the previous section. In this study, we examine how the inclusion of Compton heating affects the different accretion models ($l = 0.1\dot{m}$ and $l = 0.1\dot{m}^2$) focusing on the accretion rate and the oscillatory behaviour found in the previous works.

2.3 Radiation-hydrodynamic simulation setup

We run a suite of 1D radiation-hydrodynamic simulations for a fixed BH mass $M_{\text{bh}} = 10^6 M_{\odot}$ and a gas density $n_{\text{H},\infty} = 10 \text{ cm}^{-3}$. We use the non-relativistic hydrodynamic simulation code ZEUS-MP (Stone & Norman 1992; Hayes et al. 2006) with our 1D radiative transfer subroutine (Ricotti et al. 2001; Whalen & Norman 2006). The BH is assumed to be located at the origin of the computational domain which we cover with 256–512 logarithmically spaced radial grid zones. We assume spherical symmetry. We adopt an operator-split method that alternates hydrodynamic and radiative-transfer calculations, using the smaller of the hydrodynamical and ionization time steps at each time-step

$\Delta t = \min(\Delta t_{\text{hydro}}, \Delta t_{\text{ion}})$. The mass accretion rate is not prescribed but instead directly read at the minimum radius r_{min} at every time-step and converted to the radiation luminosity depending on the accretion model. For the radiative-transfer calculation, the number of photons in 50 logarithmically spaced energy bins from 13.6 eV to 100 keV are calculated using the instantaneous BH luminosity and the spectral index α . Our subroutine solves the 1D radiative transfer equation by calculating photo-heating/ionization, gas cooling, radiation pressures, and Compton heating as explained in Section 2.1. The Compton heating rate Γ_C is calculated directly by performing the integral shown in Equation (1). Our 1D radiative transfer subroutine updates the abundances of H I, H II, He I, He II, He III, and e^- at each radius for every time-step. We run simulations with a different spectral index in the range of $1.0 \leq \alpha \leq 1.8$ with a fixed energy range from $E_{\text{min}} = 13.6 \text{ eV}$ to $E_{\text{max}} = 100 \text{ keV}$. The spectral index α is kept constant in each simulation.

3 RESULTS

3.1 Accretion rate as a function of spectral index

Fig. 2 shows the accretion rates ($\lambda_{\text{rad}} = \dot{M}/\dot{M}_B$) as a function of time for the simulations with Compton heating included. We normalise the accretion rate to the Bondi accretion rate $\dot{M}_B = \pi e^{3/2} \lambda_B G^2 M_{\text{bh}}^2 \rho_{\infty} c_{s,\infty}^{-3}$ where λ_B is the dimensionless accretion rate assuming isothermal equation of state ($\gamma = 1$), ρ_{∞} is the density of the gas. For the assumed simulation parameters ($M_{\text{bh}} n_{\text{H},\infty} = 10^7 M_{\odot} \text{ cm}^{-3}$, $T_{\infty} = 10^4 \text{ K}$, and $\eta = 0.1$), it can be shown that $\dot{m} \sim 2.5 \lambda_{\text{rad}}$. The left panels show the model $l \propto \dot{m}$ while the right panels show the model $l \propto \dot{m}^2$. From top to bottom, the spectral index decreases ($\alpha = 1.5, 1.2$, and 1.0). Strong oscillation of the accretion rate is seen for $\alpha = 1.5$ for both models, however the oscillatory behaviour becomes suppressed with decreasing spectral index. The accretion amplitude between the maximum and the minimum decreases and the mean accretion rate (shown as dashed lines) also decreases as the spectrum becomes harder for both $l \propto \dot{m}$ and $l \propto \dot{m}^2$ models. For $l \propto \dot{m}$ model at $\alpha = 1.0$, the oscillation becomes almost completely suppressed and the mean accretion rate becomes $\sim 10^{-4}$ of the Bondi rate. Mild oscillations are observed for the model $l \propto \dot{m}^2$ at $\alpha = 1.0$ and the accretion rate becomes $\sim 10^{-3}$ of the Bondi rate, higher than the rate for the $l \propto \dot{m}$ model.

Fig. 3 shows the time-averaged accretion rate ($\langle \lambda_{\text{rad}} \rangle$) as a function of the spectral index. Different symbols show different sets of simulations: $l \propto \dot{m}$ with photo-heating only (triangles), $l \propto \dot{m}$ model with Compton heating (circles), and $l \propto \dot{m}^2$ with Compton heating (squares). The average accretion rate for the photo-heating-only model shows mild dependence on the spectral index, while the both models with Compton heating show strong dependencies on the spectral index. $l \propto \dot{m}^2$ model shows that the accretion is suppressed as the spectrum becomes harder (0.1 per cent of the Bondi rate when $\alpha \sim 1$). The average accretion rate for the model $l \propto \dot{m}^2$ shows milder dependence on the spectral index than the model $l \propto \dot{m}$ does.

3.2 Compton heating vs. photo-heating

Fig. 4 shows the distribution of the ratio between the Compton and photo-heating rates as a function of radius for $l \propto \dot{m}$ model. Since the ratio at each radius changes as a function of time (neutral fraction of H and He changes depending on the accretion luminosity)

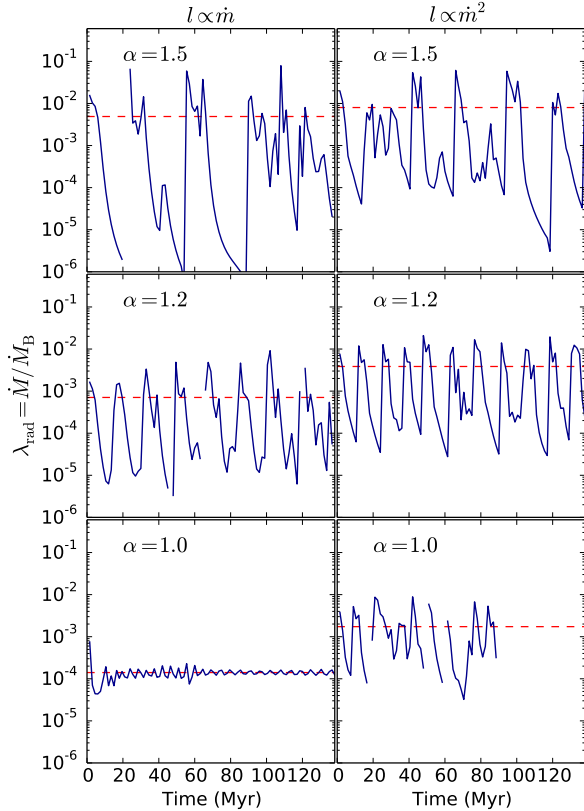


Figure 2. Evolution of the accretion rates for simulations with different spectral index ($\alpha = 1.5, 1.2$ and 1.0) for accretion models $l \propto \dot{m}$ (left panels) and $l \propto \dot{m}^2$ (right panels). λ_{rad} shown here is the accretion rate normalised by the Bondi rate (\dot{M}_B). As the Compton temperature increases with decreasing spectral index α from top to bottom panels, the accretion rate and the amplitude of the oscillations for both models decrease. For the case of $\alpha = 1.0$, oscillatory behaviour is almost suppressed for the $l \propto \dot{m}$ model, while $l \propto \dot{m}^2$ model still displays oscillation of the accretion rate. The $l \propto \dot{m}$ model shows significantly reduced time-averaged accretion rate $\langle \lambda_{\text{rad}} \rangle$, shown as a dashed line in each panel, while the $l \propto \dot{m}^2$ model displays the milder change.

due to the oscillatory behaviour of accretion, we show a 2D histogram of the combined outputs up to 135 Myr with regular time-step. Note that the relative distribution is relevant here since the number in each bin depends on the bin size and the frequency of the simulation outputs. The top panel shows the simulation with $\alpha = 1.1$ and the bottom shows the simulation with $\alpha = 1.5$. For both cases, Compton heating becomes dominant as the radial position inside the Strömgren sphere becomes nearer to the BH, while the ratio increases as a function of radius outside the Strömgren sphere (shown as narrow distribution in Fig. 4). Note that both Compton and photo-heating rates are low outside the Strömgren sphere due to the high optical depth.

The ratio of the Compton-heating and photo-heating rates as a function of radius can be explained directly by the ratio between neutral and ionized fractions as mentioned in Sec 1. Fig. 5 shows the ratio distribution between the abundances of H II and H I for the same simulations shown in Fig. 4. The Compton heating rate is proportional to the electron number density as in Equation (1)

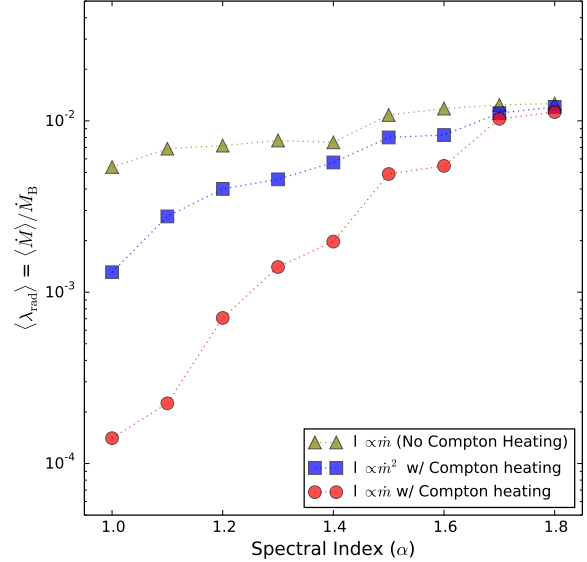


Figure 3. Time-averaged accretion rates normalised by the Bondi rate ($\langle \lambda_{\text{rad}} \rangle$) as a function of spectral index in the range $1.0 \leq \alpha \leq 1.8$ for different feedback models: $l \propto \dot{m}$ with photo-heating only (triangles), $l \propto \dot{m}^2$ with Compton heating (squares), and $l \propto \dot{m}$ with Compton heating (circles). The average accretion rate for the photo-heating only model shows a mild dependence on the spectral index while the models with Compton heating show strong dependence on the spectral index. $\langle \lambda_{\text{rad}} \rangle$ is $\sim 10^{-4}$ for the model $l \propto \dot{m}^2$ and $\sim 10^{-3}$ for the model $l \propto \dot{m}$ when $\alpha = 1$. The accretion rate for the model $l \propto \dot{m}^2$ shows intermediate dependence on the spectral index between the models $l \propto \dot{m}$ and photo-heating only.

where the ionization fraction is close to unity inside the Strömgren sphere. In contrast, the photo-heating rate is proportional to the neutral fraction of the gas, which increases as a function of radius inside the Strömgren sphere. This fact explains well the radial behaviour of the relative strength of the two heating mechanisms.

Only a tiny fraction of the H II region, more than 2 orders of magnitude smaller in radius than the I-front, is dominated by the Compton heating for $\alpha = 1.1$. Compton heating becomes more efficient at low α due to the suppressed oscillatory behaviour as shown at the top panel of Fig. 5, whereas Compton heating is dominant over photo-heating only during the peak accretion phase for $\alpha = 1.5$ (bottom panel of Fig. 5).

4 SUMMARY AND DISCUSSION

In this paper, we investigate the relative role of Compton-heating and photo-heating on radiation-regulated accretion on to BHs. We summarize our findings as follows.

- We find that the Compton heating is important when the spectrum of the BH radiation is hard ($\alpha \sim 1$) or $T_C = 3 \times 10^7$ K. The oscillatory behaviour due to the radiative feedback loop becomes weak and the average accretion rate is as well suppressed to 0.01 ($l \propto \dot{m}$ model)–0.1 ($l \propto \dot{m}^2$ model) per cent of the Bondi rate. The accretion rate increases and the oscillatory behaviour becomes stronger with increasing spectral index. When the spectrum is soft ($\alpha > 1.5$), photo-heating prevails regardless of models making the effect of Compton heating negligible.

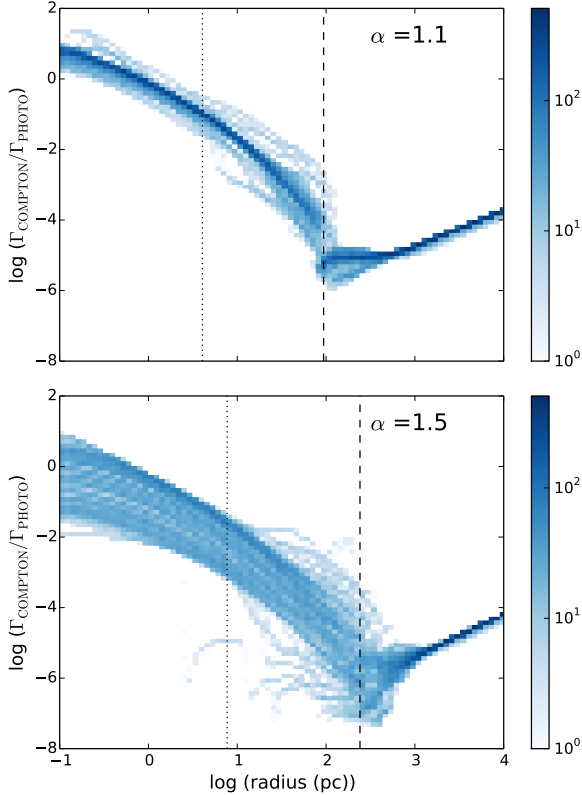


Figure 4. 2D histogram for the distribution of the ratio between Compton heating and photo-heating as a function of radius for the spectral index $\alpha = 1.1$ (top) and 1.5 (bottom). The simulation with a hard spectrum (top panel) shows less variation of the ratio compared to the one with a softer spectrum (bottom). Only at small radius does Compton heating dominate photo-heating, whereas photo-heating is the primary source of heating for the most of the volume of the Strömgren sphere. For $\alpha = 1.5$, Compton heating affects the heating dominantly only at the peak luminosity due to the strong oscillation of accretion rate. Vertical lines show the I-front (dashed) and effective accretion radius (dotted) from time-averaged profiles, respectively.

- Compton heating is important near the BH inside the Strömgren sphere, while the photo-heating still prevails in most part of the Strömgren sphere. In particular, we emphasize that the photo-heating dominates the Compton heating at the radial scale of the I-front where the gas supply to the inside the Strömgren sphere is regulated. The ratio of Compton-heating and photo-heating as a function of radius is well explained by the ratio between the ionized and neutral fraction.

- The accretion feedback model $l \propto \dot{m}^2$ shows physically consistent results with the radiatively inefficient ADAF model where the accretion rate is low and the spectrum is hard ($\alpha \sim 1$). $l \propto \dot{m}^2$ model shows intermediate results between the feedback model $l \propto \dot{m}$ and photo-heating-only model.

We limit the results of the current study to the case of accretion on to BHs from a neutral, dense, and warm medium with $T \sim 10^4$ K. When the gas is hot, ionized and optically thin as found in elliptical galaxies or at the central region of galaxy clusters, Compton heating is regarded as the critical heating mechanism for the BH feedback, especially when the spectrum is hard.

We fix the hardness of the spectrum during a simulation in the current work; however, the state transition of the BH spec-

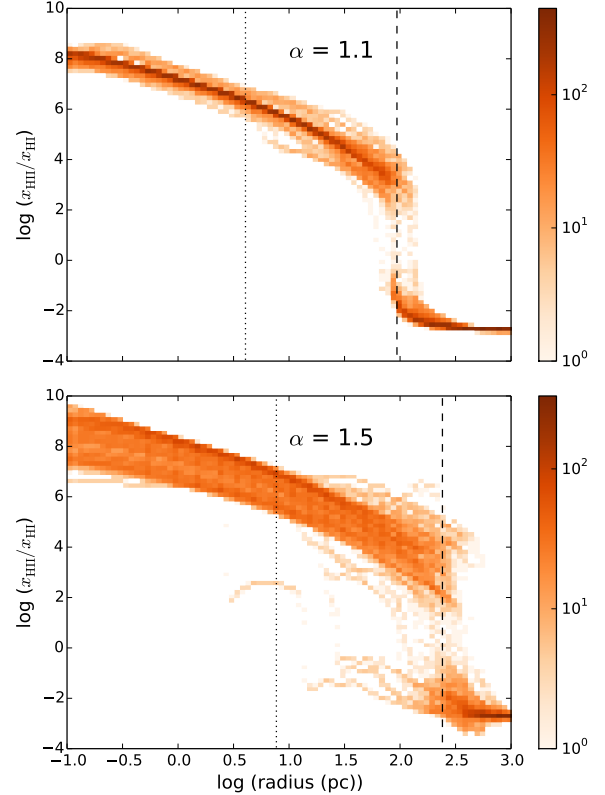


Figure 5. 2D histogram for the distribution of the ratio between the abundances of H II and H I as a function of radius for the spectral index $\alpha = 1.1$ (top) and 1.5 (bottom) for the same simulations shown in Fig. 4. The ratio between Compton heating and photo-heating as a function of radius shown in Fig. 4 can be well explained by the ratio between the ionized and neutral fractions. Same vertical lines drawn in Fig. 4 are shown.

trum should play an important role in determining the phenomena discussed here (Gan et al. 2014). Most of the gas accretion happens during the high luminosity phase where the spectrum is *soft* while the spectrum stays in a *hard* state during the low accretion phase (Yuan et al. 2009; Yuan & Narayan 2014). Dependence of the state transition on the BH luminosity should be considered in future work.

In this work, we assume an idealised power-law spectrum with a fixed energy range so that we can express the Compton temperature in an analytic manner. However, the high-energy observation of SMBHs reveals that the spectral energy distribution in the range of UV and X-ray shows a deviation from the single power-law. (Sazonov et al. 2004) found a double-peaked distribution from the weighted sum of obscured and unobscured quasar spectrum and calculated the effective Compton temperature accurately $T_C = (1.9 \pm 0.8) \times 10^7$ K. However they point out that the contribution of the blue bump to the Compton heating is less than 25 per cent, which is smaller than the error of the calculated Compton temperature. Additionally, the approximate estimation of the effective spectral slope of the averaged spectrum of the quasars in their work still falls within the range of $1 < \alpha < 1.5$. Considering the effective spectral slope and the Compton temperature, applying the double-peaked spectrum to the simulations is not likely to produce a significant qualitative difference from the current results.

ACKNOWLEDGEMENTS

The authors thank the referee, Luca Ciotti for constructive comments and positive feedback. KP is supported by the Urania E. Stott Fellowship of The Pittsburgh Foundation. This research was supported in part by the National Science Foundation under Grant No. NSF PHY11-25915 via the program *A Universe of Black Holes* hosted by the Kavli Institute for Theoretical Physics. MR's research is supported by NASA grant NNX10AH10G, NSF CMMI1125285 and ILP LABEX (under reference ANR-10-LABX-63) supported by French state funds managed by the ANR within the Investissements d'Avenir programme under reference ANR-11-IDEX-0004-02. TDM acknowledges the National Science Foundation, NSF Petapps, OCI-0749212 and NSF AST-1009781 for support. CSR and MR thank the National Science Foundation for support under the Theoretical and Computational Astrophysics Network (TCAN) grant AST1333514. This paper benefits from the private conversation with Jeremiah Ostriker. The numerical simulations in this paper were performed using the cluster facilities ("ferrari" and "coma") of the McWilliams Center for Cosmology at Carnegie Mellon University.

REFERENCES

- Abramowicz M. A., Chen X.-M., Granath M., Lasota J.-P., 1996, *ApJ*, 471, 762
- Begelman M. C., Armitage P. J., 2014, *ApJ*, 782, L18
- Belloni T. M., Motta S. E., Muñoz-Darias T., 2011, *Bulletin of the Astronomical Society of India*, 39, 409
- Blumenthal G. R., 1974, *ApJ*, 188, 121
- Bondi H., 1952, *MNRAS*, 112, 195
- Bondi H., Hoyle F., 1944, *MNRAS*, 104, 273
- Choi E., Ostriker J. P., Naab T., Johansson P. H., 2012, *ApJ*, 754, 125
- Choi E., Ostriker J. P., Naab T., Oser L., Moster B. P., 2014, *arXiv* 1403.1257
- Ciotti L., Ostriker J. P., 2001, *ApJ*, 551, 131
- Ciotti L., Ostriker J. P., 2007, *ApJ*, 665, 1038
- Ciotti L., Ostriker J. P., Proga D., 2009, *ApJ*, 699, 89
- Cowie L. L., Ostriker J. P., Stark A. A., 1978, *ApJ*, 226, 1041
- Ferrara A., Salvadori S., Yue B., Schleicher D., 2014, *MNRAS*, 443, 2410
- Gan Z., Yuan F., Ostriker J. P., Ciotti L., Novak G. S., 2014, *ApJ*, 789, 150
- Harrison F. A. et al., 2013, *ApJ*, 770, 103
- Hayes J. C., Norman M. L., Fiedler R. A., Bordner J. O., Li P. S., Clark S. E., ud-Doula A., Mac Low M.-M., 2006, *ApJS*, 165, 188
- Klein O., Nishina T., 1929, *Zeitschrift fur Physik*, 52, 853
- Li Y., 2011, *arXiv*:1109.3442
- Madau P., Efstathiou G., 1999, *ApJ*, 517, L9
- Milosavljević M., Couch S. M., Bromm V., 2009, *ApJ*, 696, L146
- Miyamoto S., Iga S., Kitamoto S., Kamado Y., 1993, *ApJ*, 403, L39
- Miyamoto S., Kitamoto S., Iga S., Negoro H., Terada K., 1992, *ApJ*, 391, L21
- Mizuta A., Kane J. O., Pound M. W., Remington B. A., Ryutov D. D., Takabe H., 2005, *ApJ*, 621, 803
- Narayan R., Mahadevan R., Quataert E., 1998, in Abramowicz M. A., Björnsson G., Pringle J. E., eds, *Theory of Black Hole Accretion Disks*. p. 148
- Narayan R., Yi I., 1995, *ApJ*, 452, 710
- Natarajan P., 2014, *General Relativity and Gravitation*, 46, 1702
- Novak G. S., Ostriker J. P., Ciotti L., 2011, *ApJ*, 737, 26
- Novak G. S., Ostriker J. P., Ciotti L., 2012, *MNRAS*, 427, 2734
- Ostriker J. P., Choi E., Ciotti L., Novak G. S., Proga D., 2010, *ApJ*, 722, 642
- Ostriker J. P., Weaver R., Yahil A., McCray R., 1976, *ApJ*, 208, L61
- Park K., Ricotti M., 2011, *ApJ*, 739, 2
- Park K., Ricotti M., 2012, *ApJ*, 747, 9
- Park K., Ricotti M., 2013, *ApJ*, 767, 163
- Park K., Ricotti M., Di Matteo T., Reynolds C. S., 2014, *MNRAS*, 437, 2856
- Park M., Ostriker J. P., 2001, *ApJ*, 549, 100
- Ricotti M., 2014, *MNRAS*, 437, 371
- Ricotti M., Gnedin N. Y., Shull J. M., 2001, *ApJ*, 560, 580
- Sazonov S. Y., Ostriker J. P., Ciotti L., Sunyaev R. A., 2005, *MNRAS*, 358, 168
- Sazonov S. Y., Ostriker J. P., Sunyaev R. A., 2004, *MNRAS*, 347, 144
- Shakura N. I., Sunyaev R. A., 1973, *A&A*, 24, 337
- Shapiro S. L., 1973, *ApJ*, 180, 531
- Shull J. M., 1979, *ApJ*, 229, 1092
- Stone J. M., Norman M. L., 1992, *ApJS*, 80, 753
- Whalen D., Norman M. L., 2006, *ApJS*, 162, 281
- Whalen D., Norman M. L., 2008a, *ApJ*, 673, 664
- Whalen D. J., Norman M. L., 2008b, *ApJ*, 672, 287
- Whalen D. J., Norman M. L., 2011, *Ap&SS*, 336, 169
- Williams R. J. R., 1999, *MNRAS*, 310, 789
- Williams R. J. R., 2002, *MNRAS*, 331, 693
- Yuan F., Narayan R., 2014, *arXiv*:1401.0586
- Yuan F., Xie F., Ostriker J. P., 2009, *ApJ*, 691, 98